



In-Silico Design and Analysis of E-Textiles for Hospital Laundry: Enhancing Tracking with Chipless RFID Tags

Müjgan Naycı Duman¹  0000-0002-6028-723X

İsmail Usta¹  0000-0002-0869-5439

Gökhan Bora Esmer²  0000-0003-2405-0777

¹Marmara University Technology Faculty Textile Engineering Department, Istanbul, Turkiye

²Marmara University Engineering Faculty Electric and Electronics Engineering Department, Istanbul, Turkiye

Corresponding Author: Müjgan Naycı Duman, mnayci@yahoo.com

ABSTRACT

In the textile industry, passive radio frequency identification (RFID) tag integration is increasing from warehouse tracking to production follow-up and healthcare applications. The proposed work introduces the in-silico design of a 30x30 mm² textile-based chipless RFID (CRFID) tag with circular transmission lines for item identification using the CST Microwave Studio application. The tag antenna was designed with stainless steel/polyester twisted yarn integrated into the polypropylene tag fabric using the embroidery technique. The antenna was tested for its readability of the embedded code in the simulations with a range of 0-20 GHz frequency band, and its Radar Cross Section (RCS) responses, return losses (S₁₁), E-field, H-field, and Farfield performances were obtained. As a result, 9-bit code capacity and 1-bit/cm² code density were achieved. The UHF antenna design simulation results demonstrated the feasibility of using textile-based materials to create a CRFID tag that was lightweight, durable, and cost-effective. The CRFID tag can store and transmit data without a chip, making it ideal for healthcare applications.

ARTICLE HISTORY

Received: 20.07.2023

Accepted: 22.01.2024

KEYWORDS

Chipless RFID, embroidered RFID tag, circular RFID antenna, conductive yarn, hospital laundry tracking, e-textiles

1. INTRODUCTION

Hospital textiles have a critical impact on infection control in hospitals, and they supply protection as a barrier to the spread of infection. Some hospitals prefer to use single-use textiles, while others prefer reusable ones. Single-use textiles benefit in labor costs; however, they have high waste disposal costs [1]. Additionally, they have 2-3 times more carbon footprint, energy, and water usage than reusable textiles [2]. Disposing of single-use hospital textiles may cause health risks, too [3]. The hazardous waste from healthcare facilities causes the risk of exposure to toxic or infectious materials during handling and manual sorting. Nevertheless, contamination in ground and surface waters is possible if those wastes are kept in improperly constructed landfills. The pathogens and toxic pollutants contaminating the disposable hospital textiles may be released into the environment. Reusable materials have more environmental benefits than single-use ones [2, 4-7]. They are sustainable, energy efficient (200–300%), and water-saving (250–330%) with less carbon footprint (200–300%) and volatile organics, and they also produce fewer

solid wastes (750%) [8, 9]. Thus, it is essential to launder and sterilize reusable hospital textiles with the approved procedures after each use.

The global medical textiles market reached about USD 13 billion in 2020 [18] and is expected to reach nearly USD 26.21 billion by 2028 [19]. Surgical gowns, staff uniforms, towels, hospital bedding, and curtains are some of the major products in the industry with significant fabric types. With a vast market potential, it is essential to solve issues like long washing life cycles, resistance to harsh washing conditions such as high temperature and pressure, and the reading performance of the smart RFID systems already used in hospital laundry management [20]. The laundry management of hospital textiles is a complex system, and it is crucial regarding patient safety and hygiene. This system has three main steps: collecting, sorting, and tracking linen status. This system is operated mainly by the hospital staff, which is very hard to deal with. Thus, it is easy to occur a lot of human errors during the processes, such as linen loss and incorrect inventory. Generally, hospitals need to reduce missing quantities and increase textiles' washing life cycles

To cite this article: Duman M N, Usta I, Esmer G B. 2024. In-Silico Design and Analysis of E-Textiles for Hospital Laundry: Enhancing Tracking with Chipless RFID Tags. *Tekstil ve Konfeksiyon*, 34(2), 162-174.

to improve the performance of their management systems. Nowadays, even hospitals want to track the laundry processes; they need to know if they are dried and ironed in the required conditions to reduce contamination or damage, besides knowing if they are washed by using the correct detergent at the correct temperature for each textile group [10-13]. So, integrating smart tags, like RFID tags, is vital for tracking the laundry, collecting data on damaged hospital textiles, and reducing staff workload for inventory management of the hospital laundry [14, 15]. The washable RFID tags have been widely used by attaching to hospital textiles and placing the readers in related places for RFID-based healthcare laundry management. RFID tags reduce the staff workload and hospital textile loss and save time and money for adoption [10, 16] in industrial laundering. Identifying cloth types also helps determine the washing program and detergent requirement accordingly [17].

RFID is a technology for identifying and tracking objects by using radio waves. An RFID system consists of four main elements: an RFID tag with an RF antenna, an integrated circuit (IC), an RFID reader, and a software application to analyze and store the information data of the tagged objects. The reader side creates and transmits a radio frequency (RF) signal to the RFID tag in the system. The RF electromagnetic field activates the tag within the reader's interrogation zone and responds with a signal to send the tag identity (ID) embedded in the chip. Finally, the reader identifies the object from the captured signal emitted by the RFID tag [21]. The reader can identify multiple RFID tags simultaneously in the environment. As shown in Figure 1, the traditional washable RFID tags use an IC that stores the information. However, the IC limits the applicability of RFID tags in laundry applications. The CRFID technology can eliminate the need for a chip to overcome the limits on applicability, making it possible to produce RFID tags at a lower cost, smaller size, and enhanced durability.

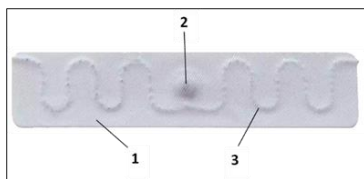


Figure 1. Components of a washable standard RFID tag: 1- two layers of tag fabric, 2- integrated circuit (IC) encapsulated between two layers of fabric, 3- UHF antenna embroidered with conductive yarn.

The RF antenna performance of a washable RFID tag depends on the antenna pattern and stitch density. Thus, different lengths of the transponders have been designed in different tag antennas to get the inductive coupling [24-34] to improve the performance of their reading ranges and reduce the tag's dimensions to decrease the costs. The laundry tags were coated with protective materials [23, 25] or encapsulated between fabric or silicon layers [14, 36] to protect the antenna and the IC from harsh washing and drying environments. The results showed that coating or

encapsulating was an excellent choice to protect the tag and the chip from moisture during the washing process; however, its resistance was insufficient to repeated washing and drying cycles, which caused mechanical stresses [23, 37].

There has been considerable work on chipless (IC-free) RFID tags [26-28, 31, 37-46], where the ID code generation was done by chipless alternative means, such as encoding by antenna design. Chipless Radio Frequency Identification (CRFID) uses electromagnetic (EM) wave transmissions and identifies objects wirelessly [48]. The CRFID system consists of the same elements as the RFID system, but the main difference is the tag antenna, whose structure is the encoding element with a unique ID and has no IC to store the ID code. The RFID reader uses an antenna to transmit the radio frequency signal to the CRFID tag. Then, the CRFID tag backscatters the coded ID information to the reader [30, 49]. Thus, the correct RFID reader and the optimum tag antenna design are essential to maximizing the reading range. Besides, the tag antenna shape and the material used in forming the antenna also significantly affect the performance of the generated CRFID; they need to be flexible and compact for wearables and textiles and durable for washing and drying processes. Silver-coated or twisted conductive yarns were primarily used in CRFID applications [26, 30, 33, 42]. Other conductive metals, like nickel or copper, were rarely used in conductive threads [29, 36, 42]. However, they all corrode over time due to exposure to water and air. Stainless steel filaments or twisted yarns can be preferred to overcome the corrosion problem [23, 25, 50].

The CRFID system mainly uses a frequency domain method to encode the data from received signals. The frequency domain method maximizes the data capacity and the reading range and guarantees high radar cross-section (RCS) responses compared to the time domain method [51, 52]. Frequency-based coding has a main principle; it shows "1" in the transmission scattering parameter (S -parameter) if there is a resonance and "0" if there is no resonance [29]. However, the number of resonators determines the data and the coding capacity of the frequency-based CRFID tag. In general, one set of resonators represents 1-bit coding data, and the main issue is improving the coding capacity without increasing the size and frequency range [29, 53-55].

The studies in the literature for laundry management were on RFID tags having chips and mostly on improving their performance and washing durability due to the limitations of an aggressive industrial laundry environment [20, 25, 26, 56-59]. However, CRFID tags have not yet been used and studied in hospital applications and item tracking. The presented work focused on developing a textile-based CRFID tag for laundry management. In this paper, a textile-based 9-bit circular CRFID tag with embroidered antennas was designed and simulated to show that CRFID tags could be used in hospital textile tracking to overcome the

problems caused by chips without compromising the tag's performance. Eliminating chips in RFID tags used in laundry management will improve the durability of the tag and prevent product losses. In the tag antenna, the resonators were designed with stainless steel twisted polyester yarn, which was durable and non-corrosive, to eliminate the coating or encapsulating processes for protection and to decrease costs. Besides, the proposed CRFID tag can be easily manufactured and orientation-independent in polarization. Additionally, it does not need a ground plane and can be embroidered directly onto hospital textiles.

2. MATERIAL AND METHOD

The dimensions of a CRFID tag depend on the tag's design and operating frequency range. However, CRFID tags typically do not have a traditional integrated circuit. They are made up of materials and structures that resonate at specific frequencies when excited by an electromagnetic wave. The physical size of a CRFID tag can be influenced by various factors, such as the number and type of resonant structures used, the substrate material, and the operating frequency range. Typically, CRFID tags operate in the microwave frequency range and can have dimensions ranging from a few millimeters to several centimeters. Some common types of CRFID tags include barcode-like, spiral, or resonant antennas. The dimensions of these tags can vary based on the specific design and frequency range and are often optimized to achieve the desired read range and sensitivity.

No standard for the operating frequency band of chipless tags has been announced yet. Therefore, a CRFID tag was proposed that operated in the 0-20 GHz frequency range to achieve high data capacity with minimum loss and maximum gain. The designed CRFID tag was shown in Figure 2 and consisted of a coded tag antenna embroidered with conductive yarn and a textile tag fabric. This CRFID tag had structurally identical nine circular resonators for 9 bits, resulting in 2^9 different ID combinations. The representation was obtained in the frequency domain. The tag antenna design had three groups of circular microstrip transmission lines with a specific configuration, and these lines represented a unique ID code. The circular design was chosen due to its symmetrical shape to obtain polarisation independent of reading direction and angle [28, 40, 42, 60]. The sharp-cornered tag antenna designs, like square or rectangle shapes, may cause unwanted scattering centers and variations in the frequency signature. The spacing between the resonators, which ranges from a few millimeters to several millimeters, can also affect the chipless RFID tag's overall dimensions and RCS response. The spacing was typically chosen to optimize the tag's sensitivity and read range.

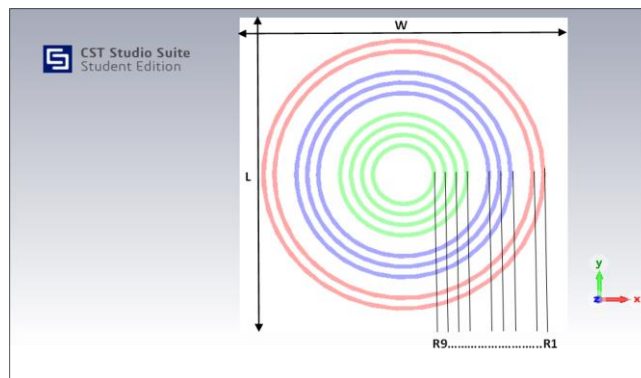


Figure 2. Design of the proposed CRFID tag with the ID code 11-111-1111 using CST Microwave Studio: W-width of the tag fabric, L-length of the tag fabric, from R1 to R9-transmission lines of the antenna.

The following steps were followed to design a CRFID tag with an operating frequency between 0-20 GHz and having circular resonators embroidered using stainless steel twisted polyester yarn:

1. The desired coding scheme was determined: The coding scheme defines the number and size of resonators required. The larger the number of resonators, the more significant the number of unique codes can be generated. For this design, a binary coding scheme was used.
2. The form and size of the resonators were determined: The form and size of the resonators are related to the desired operating frequency and coding scheme. For this design, circular resonators were arranged in a circular pattern, with one resonator in the center and eight resonators surrounding it by aligning to the center to get the tag polarized independently from direction and obtain maximum conductivity and signal strength [28, 30, 42, 47]. The width of the circular resonators was 0.4 mm, and the space between the resonators was 1 mm. In the tags with groups, the space between groups was 2 mm. Keeping the distance between resonators to a minimum was essential to avoid higher mutual coupling and have a narrower frequency bandwidth [47].
3. The materials for the substrate and antenna were chosen: According to our previous study on RFID tag fabric optimization, polypropylene fabric was used as the substrate material for the CRFID tags [61]. This tag fabric was easily found in the market and specially produced for RFID tag production. Furthermore, stainless steel twisted polyester yarn (Coats Gral AST anti-static conductive yarn) was used to embroider the antenna resonators. The 30 mm × 30 mm tag was designed with the properties listed in Table 1.
4. Tag design was parameterized: The radius of each resonator, R1, R2, R3, ..., and R9, was determined according to the tag fabric size, which was sold in standard widths (2,3,4, or 5 cm). The results for the tag fabric with a 3 cm width were presented in this study.
5. A numerical optimization for the tag was performed using CST: The tag can be optimized by adjusting the

size and position of the resonators, the substrate material, and the distances between the resonators by simulating the antenna's performance using electromagnetic simulation software CST Microwave Studio 2022 simulation application. In this study, the effect of the size and positions of the resonators were evaluated.

- Simulation of the tag was conducted: The CRFID tag was simulated within the frequency range of 0-20 GHz for its readability. RCS responses and S-parameter results were obtained using CST to optimize the antenna design. A probe was placed at a distance of 200 mm from the tag to determine the readability of the tag.

Table 1. Properties of conductive yarn and substrate used in designed CRFID tag.

Property	Materials/Measurements
Antenna shape	Circular
Conductive yarn	Stainless steel twisted polyester
Yarn count	105 Tex
Yarn conductivity	30 Ω/m
Yarn thickness	0.4 mm
Substrate	Polypropylene
Substrate thickness	0.4 mm
Substrate dielectric permittivity (ϵ_r)	2.25@868 MHz
Substrate surface resistivity	10 ¹³ Ohm/m ²
Substrate loss tangent	0.0005

In this design, periodic circular transmission lines (resonators) form closed loops to get RF waves reflected and decoded as bits assigned to the RCS [52]. RCS is a parameter to characterize backscattered signals from a tagged object, and it is extracted as a function from the signal depending on the frequency [62]. The RCS response was obtained by using transmitter and receiver antennas. Each resonator in the tag antenna formed a frequency signature with a peak for 1-bit data. When communication between the reader and the tags is established, the load impedance of the tag changes, and this modulates the RCS of the tag. The RCS of a backscattered signal is the equivalent area of the signal depending on whether the signal re-emits or scatters the incident power isotropically. The RCS of a signal does not refer to its physical size, but it shows how effectively the signal can distribute its power. The deeper the tag modulates the RCS, the longer the connection range from tag to reader will be.

The 3D model of the tag design was simulated by the CST Microwave Studio. The topology of the circular resonators obtained by embroidering the conductive yarns can be seen in the cross-sectional view of the tag in Figure 3. There was no integrated microchip to control the information exchanged between the tag and the reader as in chip-based RFID tag systems. Still, the ID could be identified by analyzing the backscattered signal from the tag. Eliminating the need for a chip made the developed CRFID tags safer for attackers and cost-effective. Based on the substrate of the tag and materials used in the antenna, the performance

of the CRFID tag could be satisfied in the laundry process with long durability.

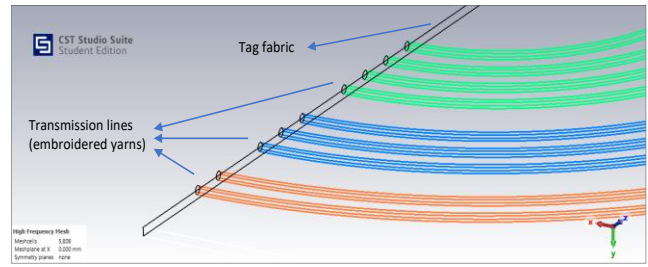


Figure 3. Cross-sectional view of the chipless RFID tag proposed in this work.

The reading system uses the tag data decoded from the backscattered signal to create a tag ID according to general electronic product code (EPC) standards. The designed chipless RFID tags had fewer ID bits than the RFID tags with chips that limited the number of unique IDs created for the RFID tags. The number of unique IDs is directly proportional to 2 over several ID bits. For example, a 3-bit ID code creates 2³ (eight) different RFID tag IDs. Bit density is the ratio of the number of data bits encoded per tag's unit area, and it was calculated for the designed and simulated CRFID tag with Equations (1), (2), and (3) as 1 bit/cm² [28]. Higher bit density means having higher coding bit capacity and smaller tag size with lower costs. There are three essential factors for determining the bit density: the tag dimensions, using the bandwidth efficiently, and choosing the correct encoding technique that is most effective.

$$\text{Bit Density (bits/cm}^2\text{)} = \text{Code Capacity} / \text{Tag Size} \quad (1)$$

$$2^{\text{Code Capacity}} = \text{Combinations}_{\text{Total}} \quad (2)$$

In the presented study, there were three groups of resonators: the first group had two resonators R1 and R2; the second group had three resonators R3, R4, and R5; and the third group had four resonators R6, R7, R8, and R9. These groups were defined from outside to inside. For each group, the combinations were calculated using Equation (3) for a laundry firm:

$$\text{Total combinations} = (\text{Number of companies}) \times (\text{Product type}) \times (\text{Product property}) \quad (3)$$

The number of companies was assumed to be sixteen, product type was assumed to be eight, and product property was taken as four. Hence, the number of total combinations, code capacity, and bit density were calculated as follows:

$$\text{Total combinations} = 16 \times 8 \times 4 = 512$$

$$2^{\text{Code Capacity}} = 512$$

$$\text{Code capacity} = 9 \text{ bits}$$

$$\text{Bit density} = 9 \text{ bits} / (3 \text{ cm} \times 3 \text{ cm}) = 1 \text{ bit/cm}^2$$

In a tag, the bit density can be increased by increasing the number of resonators and decreasing the spaces between

the resonators on the antenna without changing the tag dimensions. In this study, the design was based on embroidering the resonators onto the tag fabric, and the thickness of the yarn determined the space between the resonators. However, it will be possible to get more resonators for the same tag dimension by printing them instead of embroidering them.

In the configuration discussed above, a probe was placed 200 mm away from tags in the simulation. Mobile or located readers can be used for large-scale tag deployment in real-life measurements. The designed 11-111-1111 tag ID can be seen in Figure 2. This model divided the tag deployment field into groups, each assigned to a unique ID. A reader moved closer to a tag, read the coded tag ID, and constructed an RFID tag data frame. In the hospital laundry process, there are several group items to be stored. These groups can correspond to the company name, product type, and product property from the inside to the outside of the circular microstrip lines. For example, in an ID code 10-101-0101, the last four digits "1010" indicated the company that the product belonged to, while the second group had three digits "101" indicating the product type, such as duvet cover or pillowcase, and the first two digits "01" showed the property of the product like double or single. However, if two same tags are deployed simultaneously, the reader cannot uniquely identify the tags. If desired, two or more similar tags can be deployed in a company by increasing the number of groups on antenna design. However, the tag's size will increase when the number of groups increases. The size of the tag determines the cost and performance of the system.

Electromagnetic waves are a combination of electric and magnetic (or electromagnetic) fields propagating through space. A plane wave is one of the most straightforward solutions of the propagating electromagnetic wave equation. The plane wave propagates in space, and the direction of its E-field shows polarization. We have vertical polarization when the E-field oscillates in the X-axis and is polarized along the X-axis. On the other hand, when the E-field oscillates in the Y-axis and is polarized along the Y-axis, we have horizontal polarization [63]. In a spherical coordinate system, three more factors indicate the three axes. These are theta (θ) and phi (ϕ), which are spherical angles of the incident plane, and the distance parameter of the E-field vector (r) [64]. A point is shown on a spherical coordinate system in Figure 4a to define the coordinates with these components. A plane wave can be defined as a theta or phi-polarized plane wave, as shown in Figures 4b and 4c. The direction of the E-field is parallel to the theta's unit vector in theta polarized plane wave. In Figure 5, theta (θ)=0 and phi (ϕ)=0, and also, the propagation vector (k) is parallel to the antenna's normal incidence. By changing θ and ϕ , different RCS values can be obtained. In the CST simulation application, the antenna was designed with θ -polarized plane wave for $\theta = 0$ and simulated. In the simulation, Farfield and antenna properties were chosen for

parameterized plane wave parameters and were listed in Table 2. A time domain solver with -40 dB accuracy, hexahedral mesh type, and 50 Ohm impedance was chosen.

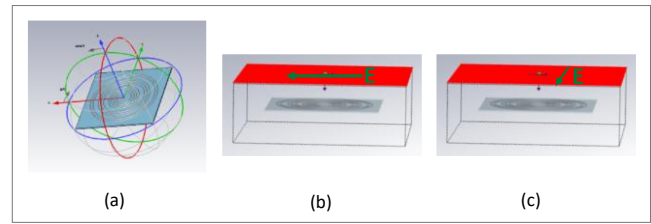


Figure 4. Spherical coordinate system (a), theta (θ) polarized (b), and phi (ϕ) polarized plane wave (c).

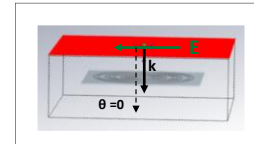


Figure 5. Polarization of plane wave when theta (θ)=0 and phi (ϕ)=0.

Table 2. Plane-wave parameters in simulation.

Property	Value
Farfield monitor	Farfield Broadband
Output data type	1D cartesian
Frequency range	0-20 GHz with 0.1 step size
theta (θ)	0
phi (ϕ)	0
Plot mode	dB scale
Source type	Plane-wave
Boundaries	Open

3. RESULTS AND DISCUSSION

In the simulation, a probe was defined with field type RCS in the cartesian coordinate system with position $(x, y, z) = (0, 0, 200)$. Farfield, E-field, H-field, and current density monitors were obtained from the simulation.

The scattering mechanism on the circular textile-based CRFID tag can be seen in Figure 6. A transmitted E-field hit the resonators, and a surface current occurred on all resonators, and then the resonators reflected the E-field from the tag. E-field on the resonators depends on the resonator lengths, and so their radiuses. As a result of the whole structure of the tag, it created a specific frequency response. The interactions of neighboring rings determined the total response, and the gaps between the resonators made the desired changes in the RCS response.

The resonators on the tag caused radiating effects. In the plane wave simulation, the Farfield radiation patterns of the proposed tag are shown in Figure 7. It can be concluded that the radiated energy can be neglected.

E-field and H-field were calculated at 8 GHz and illustrated in Figures 8 and 9, respectively. As expected, the magnitudes of electric and magnetic fields decreased with increasing distance from the center.

The CRFID antenna behaved as a frequency-selective filter when a plane wave stimulated the circular microstrip resonators. Thus, deep peaks were formed at the resonant frequencies of the resonators. As seen in Figure 10, the backscattered signal from the tag having nine resonators, which were presented with “1” in the ID code, showed nine frequency signatures and made deep resonant peaks in the

frequency response at different resonant frequencies. As RCS was a function of backscattered signal and frequency, it could be concluded that nine deep peaks were successfully obtained corresponding to each resonator of the proposed tag antenna. This means that the proposed tag antenna was functioning to identify the attached hospital textile.

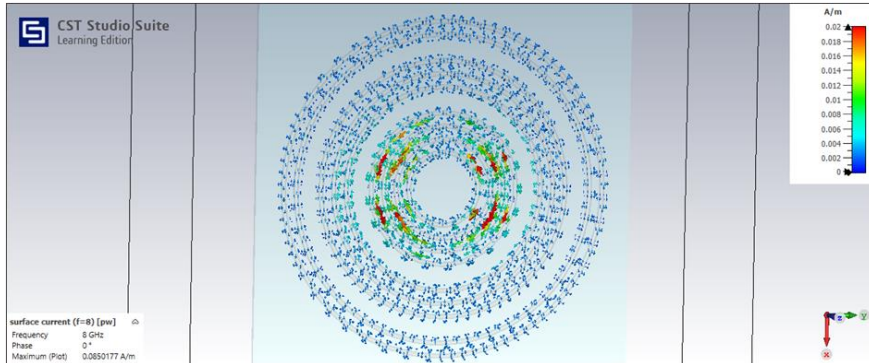


Figure 6. Surface current on the resonators at frequency 8 GHz.

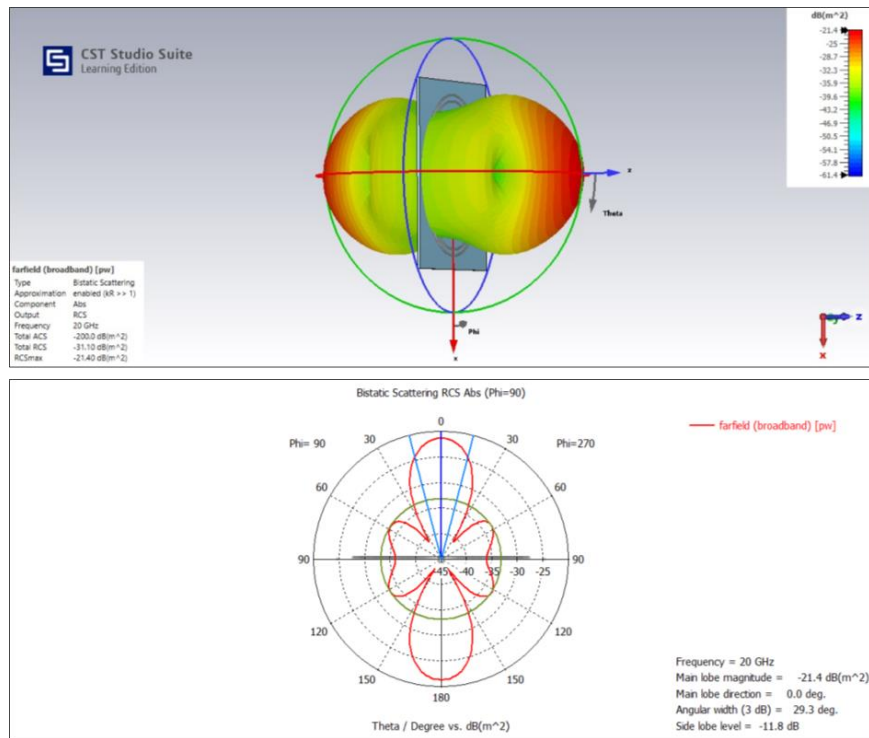


Figure 7. 3D and 1D Farfield (broadband) radiation pattern of the CRFID tag antenna.

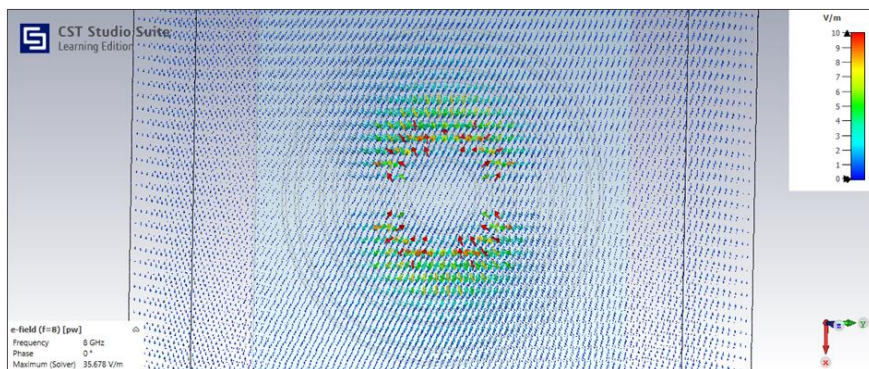


Figure 8. E-field density on the resonators at 8 GHz.

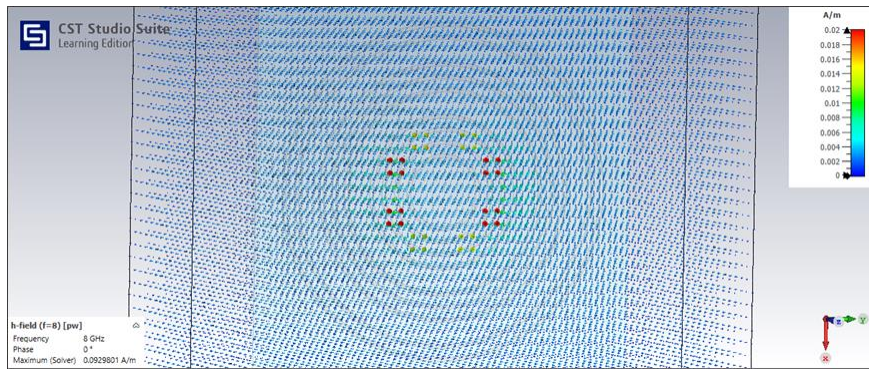


Figure 9. H-field density on the resonators at 8 GHz.

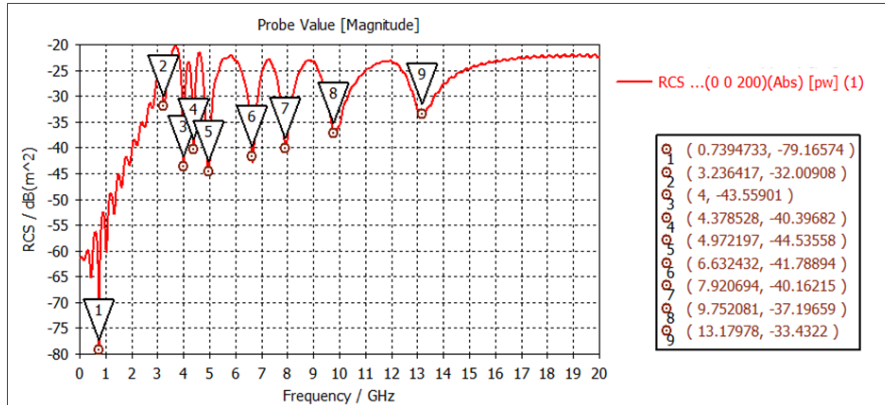


Figure 10. RCS responses for the CRFID tag with ID codes 11-111-1111.

Two different ID codes, 11-111-1111 and 10-101-0101, were designed and simulated to determine the circular chipless RFID tag's performance and verify the coding methodology's feasibility, as shown in Figure 11.

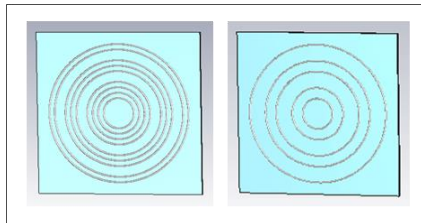


Figure 11. Circular chipless RFID tag designs with ID codes 11-111-1111 and 10-101-0101 from left to right, respectively.

The RCS responses of both the ID codes 11-111-1111 and 10-101-0101 can be seen in Figure 12. The removed resonators did not have a resonant frequency; in other words, they had "0" resonant frequencies. Having no resonant frequency meant these resonators had no reflected signal and RCS response for these resonators, so the graphic had no deep peak for them.

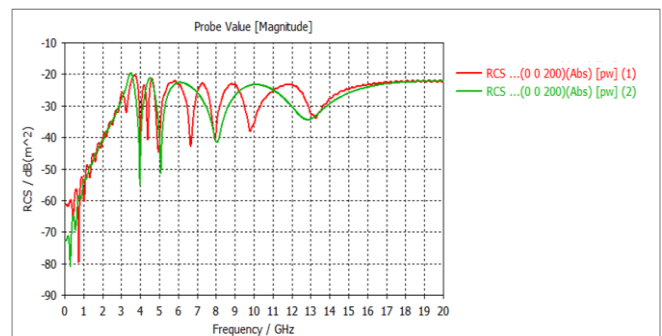


Figure 12. RCS responses for the CRFID tag with ID codes 11-111-1111 (1) and 10-101-0101 (2).

The Farfield radiation patterns of the proposed tag with the ID code 10-101-0101 are shown in Figure 13. RCSmax and RCS total values were obtained as -22.50 dB(m²) and -32.19 dB(m²) for the ID code 10-101-0101 while they were -21.40 dB(m²) and -31.10 dB(m²) for the ID code 11-111-1111, respectively. Additionally, evaluation of the effect of grouping the resonators with the same ID codes was designed and simulated without grouping and with no gaps between the groups, as shown in Figure 14. The space between the resonators was kept the same as 1mm.

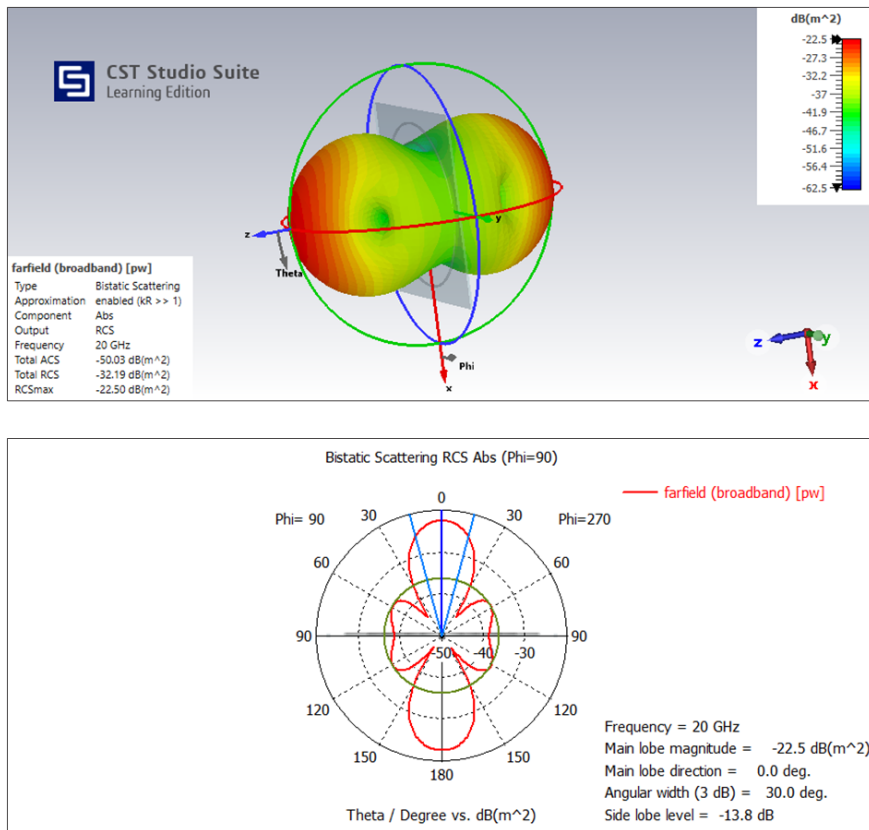


Figure 13. 3D and 1D Farfield (broadband) radiation pattern of the CRFID tag antenna with the ID code 10-101-0101.

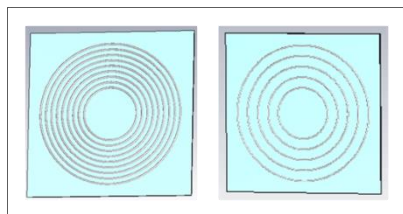


Figure 14. Circular chipless RFID tag designs with ID codes 11111111 and 101010101 from left to right, respectively.

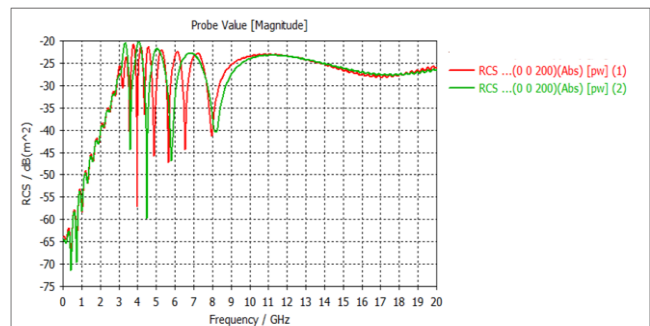


Figure 15. RCS responses for the CRFID tag with ID codes 11111111 (1) and 101010101 (2).

In Figure 15, the RCS responses of both tag antennas having ungrouped resonators with the ID codes 11111111 and 101010101 can be seen. The same RCS response pattern was obtained with the antennas grouped, but the maximum operating frequency decreased from 14 to 9 GHz due to the increasing diameters of the inner resonators. Resonator R1, with a diameter of 26 mm, was the same for both grouped and not grouped antennas. However, the diameters of the other eight resonators were changed accordingly for the ungrouped antenna. To make a cost-effective design, grouping can be used without leaving space between the groups in the antenna design, and then the frequency range can be decreased.

In Figure 16, RCSmax and RCStotal values were obtained as -24.60 dB(m²) and -32.63 dB(m²) for the ID code 11111111, while they were -25.45 dB(m²) and -33.61 dB(m²) for the ID code 101010101 as in Figure 17, respectively.

The presented study demonstrated the electromagnetic performance and feasibility of using textile-based materials to create a chipless RFID tag to provide successful results. The structure of the tag antenna contained nine resonators to generate nine resonance peaks with a capacity of the 9-bit data code. Due to the small distances between resonators in each group and high mutual coupling, the resonators behaved like a single resonator [28, 42]. The proposed tag design had all the measured resonances within the predefined frequency band. Finally, the resonant peaks were measured with RCS responses between -33.61dB and -21.40 dB with a bandwidth of 0-20 GHz.

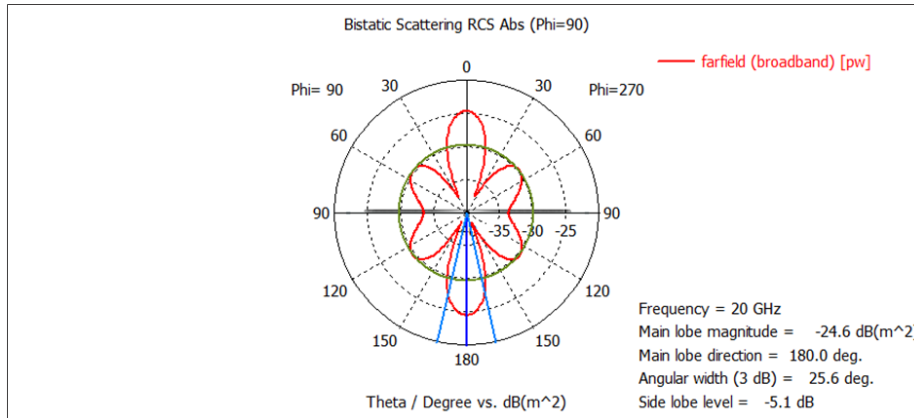
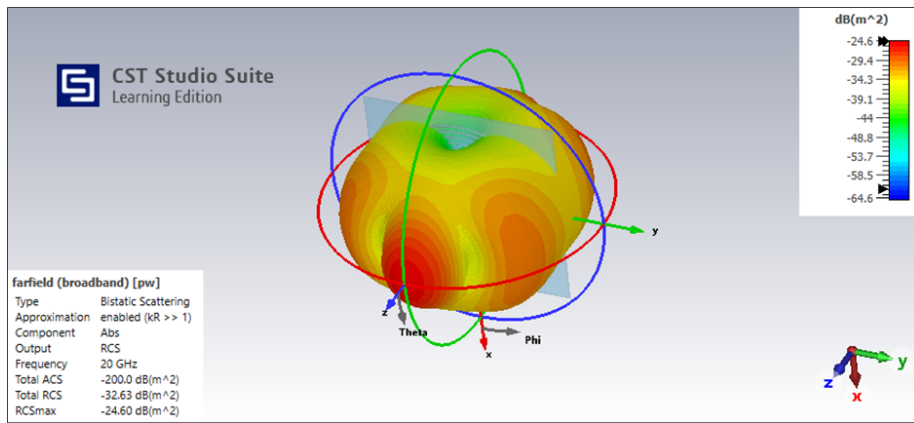


Figure 16. 3D and 1D Farfield (broadband) radiation pattern of the CRFID tag antenna with the ID code 11111111.

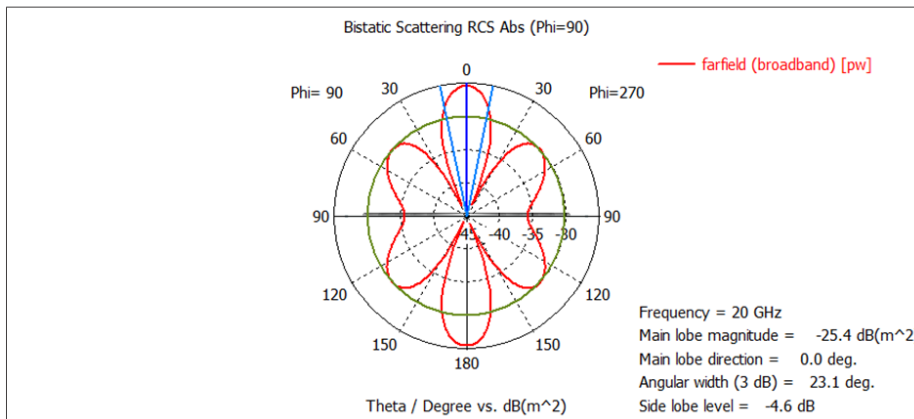
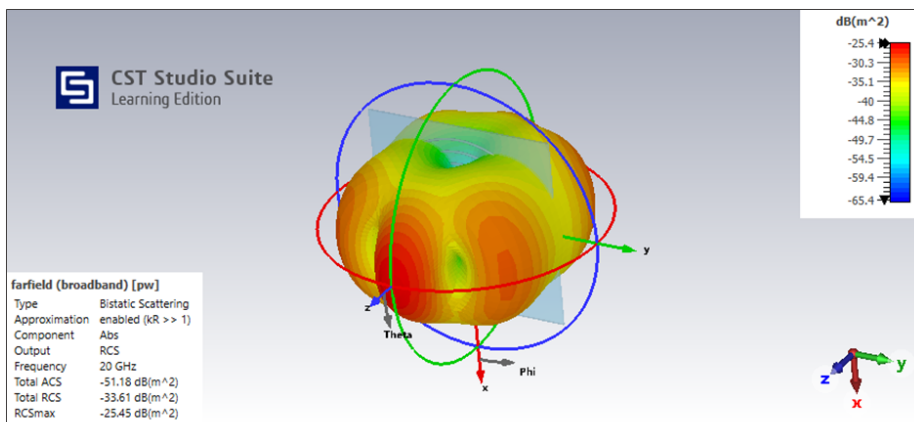


Figure 17. 3D and 1D Farfield (broadband) radiation pattern of the CRFID tag antenna with the ID code 10101010.

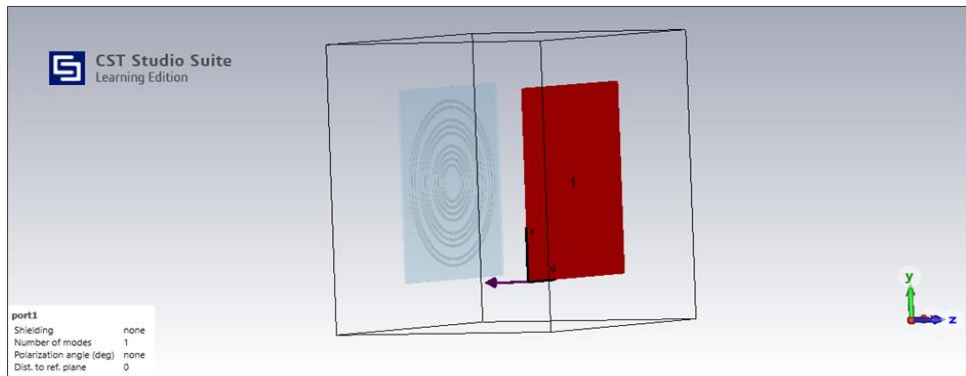


Figure 18. Waveguide port setup for nearfield measurements.

For nearfield calculations, the circular CRFID tags were located 20 mm away from the waveguide port with a 0-20 GHz bandwidth that was linearly polarized. The setup of the waveguide port can be seen in Figure 18. The return losses (S-parameter) obtained in the simulation are shown in Figures 19 and 20. The comparison of grouping or not grouping the resonators is shown in Figure 20. The resonating frequency range was 2.9-13.1 GHz for the tags with grouped resonators and 2.9-8.6 GHz for those with ungrouped resonators due to the increasing diameters of the inner resonators. The antenna design can be adjusted according to the needed working frequency range by increasing or decreasing the radii of the resonators to get a cost-effective design.

Another study was conducted to determine the performance of the CRFID tag when it was bent with the garment sewn

on. The tag with the ID 11-111-1111 was designed in CST Microwave Studio with several bending angles (20°, 40°, 60°, and 80°) and then simulated in the same conditions with the unbent tag. It can be seen in Figures 21, 22, 23, and 24 that the tag performances were affected by changing the bending angle. An increase in RC values occurred with increasing bending angles [52].

The peaks on the RCS values for all resonators were obtained in a similar design with the unbent tag regardless of the bending angle when compared to the results of the unbent tag in Figure 10. Although there was no degradation in the signals, the backscattered power was reduced, and the signals of the adjacent resonators began to interface, as seen in Figure 24. Nevertheless, the tag ID was successfully received in the simulations when the tag was bent at four different angles.

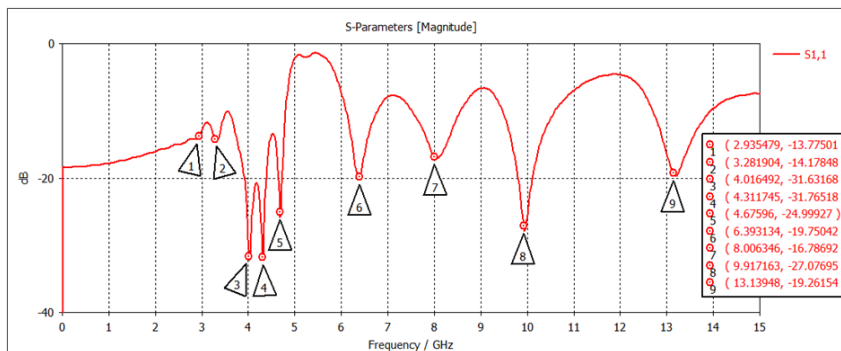


Figure 19. Simulated return losses (S-parameter) for the tags with the ID code 11-111-1111.

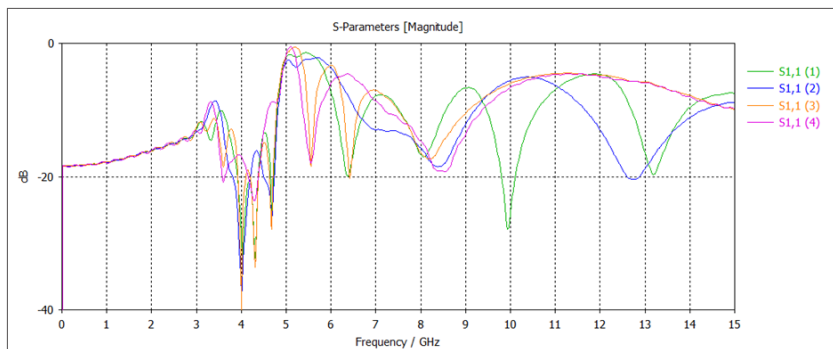


Figure 20. Simulated return losses (S-parameter) for the tags grouped and ungrouped with the ID codes 11-111-1111 (1), 10-101-0101 (2), 1111111111 (3), and 101010101 (4), respectively.

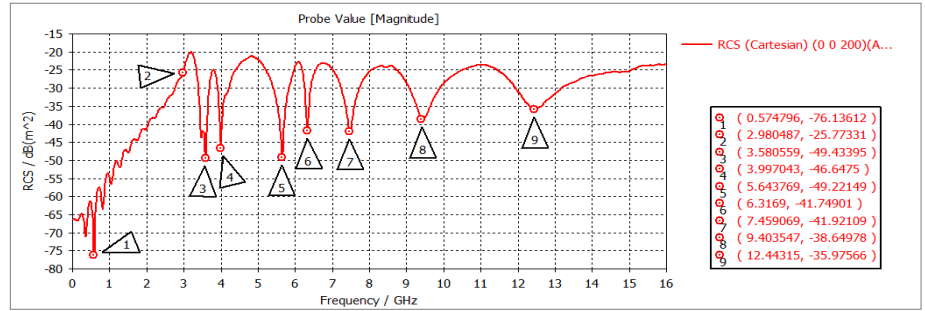
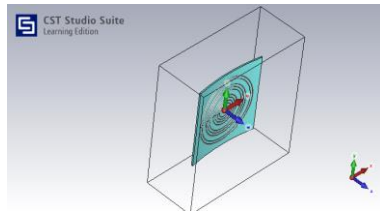


Figure 21. RCS responses for the 20° bent CRFID tag with ID codes 11-111-1111.

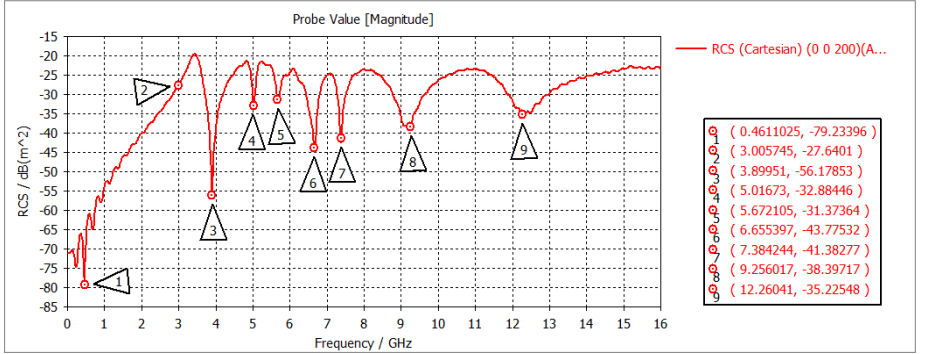
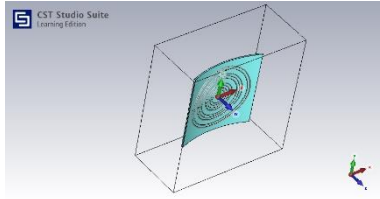


Figure 22. RCS responses for the 40° bent CRFID tag with ID codes 11-111-1111.

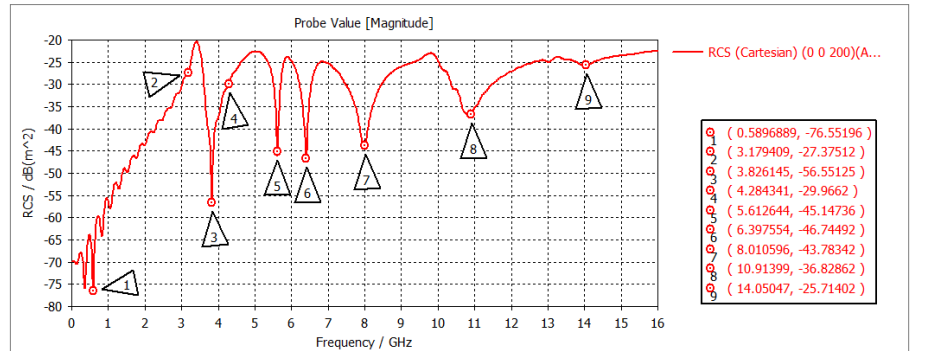
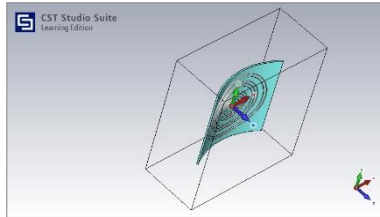


Figure 23. RCS responses for the 60° bent CRFID tag with ID codes 11-111-1111.

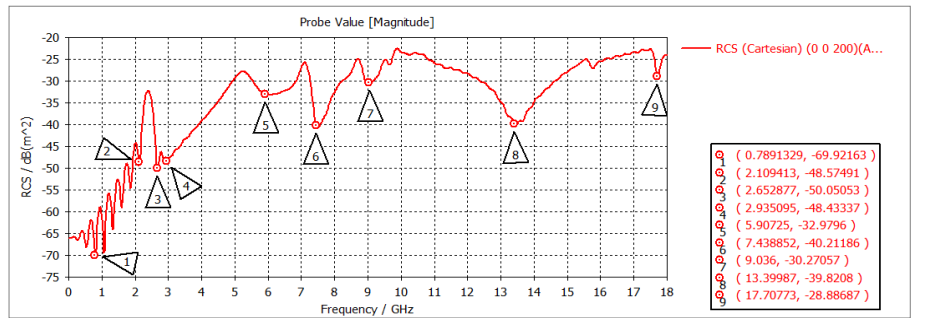
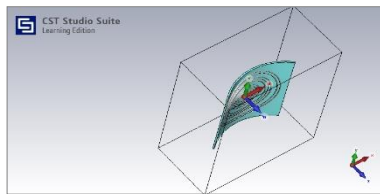


Figure 24. RCS responses for the 80° bent CRFID tag with ID codes 11-111-1111.

4. CONCLUSION

This work proposes a textile-based circular CRFID tag antenna design using the stainless-steel twisted polyester conductive yarn embroidered on polypropylene tag fabric, which was commercially available and inexpensive. A coding capacity of 9-bits was obtained with a 30×30 mm² surface area using a set of circular resonators to prove the

design. However, it is possible to enlarge the number of bits due to the parameters needed to track. Additionally, the performance of the tag was analyzed and verified for several bending conditions.

In the antenna design, grouping the resonators can allow a decrease or increase in the spaces between the resonators for needed groups according to the parameters to code in

that group. The proposed circular CRFID tag antenna design did not need an integrated circuit (IC) to operate and save the data. Moreover, it is easy to produce with an embroidery machine onto a tag fabric or directly onto the garment. Due to its lower costs and similar performance to IC tags, it can be preferred to the regular RFID tags with integrated circuits used in laundries nowadays.

The development of a textile-based CRFID tag has the potential to improve the healthcare laundry industry. The tag can be easily integrated into clothing and other hospital textiles, seamlessly tracking and monitoring data. This research will improve CRFID technology and provide a practical solution, especially for laundry applications.

The simulation results show that the CRFID tag approach can be implemented with computer simulations mimicking

the RFID tag. The simulation results provide valuable insights into the expected outcome of complex CRFID application processes. Furthermore, the antenna design exhibited a significant reading characteristic in polarization insensitivity and functioned in the 0-20 GHz frequency band.

Despite the superior results in simulation, the performance of the tags needs to be experimentally verified and compared with the simulations for different ID codes obtained in terms of RCS response and S-parameter. The coding capacity and reading range of the fully textile CRFID tag can be improved by using different materials and topologies of the antennas.

REFERENCES

- Watson D, Fisher-Bogason R. 2017. *Greener textiles in hospitals: Guide to green procurement in the healthcare sector*. Copenhagen, Denmark.
- Overcrash M. 2012. A comparison of reusable and disposable perioperative textiles sustainability state-of-the-art 2012. *Anesthesia & Analgesia*, 14(5), 1055–1066.
- WHO. 2018. Health-care waste. World Health Organization, Geneva.
- Carre A. 2008. Life cycle assessment comparing laundered surgical gowns with polypropylene-based disposable gowns. RMIT University, Melbourne, Australia.
- Mikusinska M. 2012. Comparative life cycle assessment of surgical scrub suits: the case of reusable and disposable scrubs used in Swedish healthcare.
- Burguburu A, Tanné C, Bosc K, Laplaud J, Roth M, Czyrnek-Delètre M. 2022. Comparative life cycle assessment of reusable and disposable scrub suits used in hospital operating rooms. *Cleaner Environmental Systems*, 4, 100068.
- McQuerry M, Easter E, Cao A. 2021. Disposable versus reusable medical gowns: A performance comparison. *American Journal of Infection Control*, 49(5), 563–570.
- Murphy F, Tchetchik A, Furxhi I. 2020. Reducing healthcare-associated infections (HAIs) with antimicrobial inorganic nanoparticles incorporated in medical textiles: An economic assessment. *Nanomaterials*, 10(5), 999–1012.
- Overcash MR, Sehulster LM. 2022. The estimated incidence rate of healthcare-associated infections (HAIs) linked to laundered reusable healthcare textiles (HCTs) in the United States and the United Kingdom over a 50-year period: Do the data support the efficacy of approved laundry practices? *Infection Control and Hospital Epidemiology*, 43, 1510–1512.
- Woradit K, Sassananan S, Boonjun S, Boonpratong A. 2020. Integrated RFID aperture and washing chamber shielding design for Real-Time cleaning performance monitoring in healthcare laundry system. In Proceedings of the 2019 International Conference on Biomedical and Health Informatics (IFMBE) (235–242). Lin K, Magjarevic R, de Carvalho P (eds). Taipei, Taiwan.
- UK Department of Health. 2016. Health technical memorandum 01-04: decontamination of linen for health and social care. Engineering, Equipment and Validation. London.
- Fijan S, Cencic A, Turk SŠ. 2006. Hygiene monitoring of textiles used in the food industry. *Food Microbiology*, 37(3), 356–361.
- Owen L, Laird K. 2020. The role of textiles as fomites in the healthcare environment: A review of the infection control risk. *PeerJ*, 8, e9790.
- Salayong K, Phaebua K, Lertwiriayaprapa T, Boonpoonga A, Chaiyasang L, Kumjinda A. 2019. Linen laundry management system in hospital by using UHF-RFID. In Proceedings of the 2019 Research, Invention, and Innovation Congress (RI2C) (1–4). Bangkok, Thailand.
- Ünal ZB, Dirgar E, Eda Acar, Kansoy O. 2017. A study on tracking of textile products used in hotel businesses. *Journal of Tourism Theory and Research*, 3(1), 9–15.
- Fisher JA, Monahan T. 2012. Evaluation of real-time location systems in their hospital contexts. *International Journal of Medical Informatics*, 81(10), 705–712.
- Bouet M, Pujolle G. 2010. RFID in eHealth systems: Applications, challenges, and perspectives. *Annales des Telecommunications/Annales de Telecommunications*, 65(9–10), 497–503.
- Expert Market Research. 2021. Medical Textiles Market Size, Share, Growth, Trends, Forecast 2017-2027. Wyoming, USA.
- Grand View Research. 2021. Medical Textiles Market Size, Share & Trends Analysis Report By Product (Non-woven, Woven), By Application (Healthcare & Hygiene Products, Implantable Goods), By Region, And Segment Forecasts, 2021 - 2028. Dublin, Ireland.
- Moraru A, Helerea E, Ursachi C. 2018. RFID passive tags for harsh industrial environments. *Bulletin of the Transilvania University of Brasov, Series I: Engineering Sciences*, 11(1), 39–46.
- Dobkin D, Dobkin DM. 2007. *The RF in RFID: Passive UHF RFID in Practice*. Burlington, MA.
- Moraru A, Helerea E, Ursachi C, Călin MD. 2017. RFID system with passive RFID tags for textiles. In Proceedings of the 2017 10th International Symposium on Advanced Topics in Electrical Engineering (ATEE) (410–415). Bucharest, Romania.
- Moraru A, Helerea E, Ursachi C. 2018. Passive RFID tags for textile items-requirements and solutions. In Proceedings of the 2018 International Symposium on Fundamentals of Electrical Engineering, ISFEE (1–6). Bucharest, Romania.
- López TS. 2011. RFID and sensor integration standards: State and future prospects. *Computer Standards and Interfaces*, 33(3), 207–213.
- Moraru A, Ursachi C, Helerea E. 2020. A new washable UHF RFID tag: Design, fabrication and assessment. *Sensors*, 20(12), 1–17.
- Toivonen M, Bjorninen T, Sydanheimo L, Ukkonen L, Rahmat-Samii Y. 2013. Impact of moisture and washing on the performance of embroidered UHF RFID tags. *IEEE Antennas and Wireless Propagation Letters*, 12, 1590–1593.
- Luo C, Gil I, Fernández-García R. 2022. Experimental comparison of three electro-textile interfaces for textile UHF-RFID tags on clothes. *AEU - International Journal of Electronics and Communications*, 146, 154137.

28. Tariq N, Riaz MA, Shahid H, Khan MJ, Amin Y, Tenhunen H. 2022. A novel kite-shaped chipless RFID tag for low-profile applications. *IETE Journal of Research*, 68(3), 2149–2156.
29. Corchia L, Monti G, De Benedetto E, et al. 2020. Fully-textile, wearable chipless tags for identification and tracking applications. *Sensors*, 20(2), 429–443.
30. Khan MUA, Raad R, Foroughi J, Theoharis PI, Liu S, Masud J. 2020. A silver-coated conductive fibre HC12 sewed chipless RFID tag on cotton fabric for wearable applications. In Proceedings of the 2020 IEEE 23rd International Multi-Topic Conference, INMIC (1–5). Bahawalpur, Pakistan.
31. Ali Khan MU, Raad R, Foroughi J. 2020. Transient response & electromagnetic behaviour of flexible bow-tie shaped chip-less RFID tag for general IoT applications. *Advances in Science, Technology and Engineering Systems Journal*, 5(5), 757–764.
32. Andriamiharivolamena T, Vena A, Perret E, Lemaitre-Auger P, Tedjini S. 2014. Chipless identification applied to human body. In Proceedings of the 2014 IEEE RFID Technology and Applications Conference (RFID-TA) (241–245). Tampere, Finland.
33. Vena A, Moradi E, Koski K, et al. 2013. Design and realization of stretchable sewn chipless RFID tags and sensors for wearable applications. In Proceedings of the 2013 IEEE International Conference on RFID (RFID) (176–183). Orlando, FL, USA.
34. Mishra DP, Das TK, Behera SK. 2020. Design of a 3-bit chipless RFID tag using circular split-ring resonators for retail and healthcare applications. In Proceedings of the 2020 IEEE 26th National Conference on Communications (NCC) (10–13). Kharagpur, India.
35. Mishra DP, Kumar Das T, Sethy P, Behera SK. 2019. Design of a multi-bit chipless RFID tag using square split-ring resonators. In Proceedings of the 2019 IEEE Indian Conference on Antennas and Propagation (InCAP) (1–4).
36. Kiourti A, Volakis JL. 2014. Stretchable and flexible E-fiber wire antennas embedded in polymer. *IEEE Antennas and Wireless Propagation Letters*, 13, 1381–1384.
37. Pei J, Fan J, Zheng R. 2021. Protecting wearable UHF RFID tags with electro-textile antennas: The challenge of machine washability. *IEEE Antennas and Propagation Magazine*, 63(4), 43–50.
38. Mekki K, Necibi O, Dinis H, Mendes P, Gharsallah A. 2021. Frequency-spectra-based high coding capacity chipless RFID using an UWB-IR approach. *Sensors*, 21(7), 2525–2541.
39. Iqbal MS, Shahid H, Riaz MA, Rauf S, Amin Y, Tenhunen H. 2017. FSS inspired polarization insensitive chipless RFID tag. *IEICE Electronics Express*, 14(10), 1–6.
40. Islam MA, Yap Y, Karmakar N, Azad AKM. 2012. Orientation independent compact chipless RFID tag. In Proceedings of the 2012 IEEE International Conference on RFID-Technologies and Applications, RFID-TA 2012 (137–141). Nice, France.
41. Babaeian F, Karmakar NC. 2020. Time and frequency domains analysis of chipless RFID back-scattered tag reflection. *IoT*, 1(1), 109–127.
42. Khan MUA, Raad R, Foroughi J. 2020. A fibre embroidered chipless RFID tag on cotton fabrics for wearable applications. In Proceedings of the 2020 IEEE Global Communications Conference, GLOBECOM (1–6). Taipei, Taiwan.
43. Corchia L, Monti G, Tarricone L. 2019. A frequency signature RFID chipless tag for wearable applications. *Sensors*, 19(3), 494–505.
44. Tedjini S, Boularess O, Andriamiharivolamena T, Rmili H, Aguilu T. 2017. A novel design of chipless RFID tags based on alphabets. In Proceedings of the 2017 IEEE MTT-S International Microwave Symposium (IMS) (1561–1563). Honolulu, HI, USA.
45. Betancourt D, Barahona M, Haase K, Schmidt G, Hubler A, Ellinger F. 2017. Design of printed chipless-RFID tags with QR-code appearance based on genetic algorithm. *IEEE Transactions on Antennas and Propagation*, 65(5), 2190–2195.
46. Prabavathi P, Subha Rani S. 2021. Flower shaped frequency coded chipless RFID tag for low cost item tracking. *Analog Integrated Circuits and Signal Processing*, 109(1), 79–91.
47. Sai DM, Mishra DP, Behera SK. 2021. Frequency shift coded chipless RFID tag design using square split ring resonators. In Proceedings of the 2021 IEEE 2nd International Conference on Range Technology (ICORT) (13–16). Chandipur, Balasore, India.
48. Zou Z, Shao B, Zhou Q, et al. 2012. Design and demonstration of passive UWB RFIDs: Chipless versus chip solutions. In Proceedings of the 2012 IEEE International Conference on RFID-Technologies and Applications (RFID-TA) (6–11). Nice, France.
49. Jalil MEB, Rahim MKA, Mohamed H, et al. 2021. High capacity and miniaturized flexible chipless RFID tag using modified complementary split ring resonator. *IEEE Access*, 9, 33929–33943.
50. Şamlı BE, Bahadır Ünal Z. 2018. Giysi üretiminde iletken kumaşların kullanımı. *Mesleki Bilimler Dergisi (MBD)*, 7(3), 445–451.
51. Abdulkawi WM, Sheta AFA. 2019. K-state resonators for high-coding-capacity chipless RFID applications. *IEEE Access*, 7, 185868–185878.
52. Betancourt D, Haase K, Hübler A, Ellinger F. 2016. Bending and folding effect study of flexible fully printed and late-stage codified octagonal chipless RFID tags. *IEEE Transactions on Antennas and Propagation*, 64(7), 2815–2823.
53. Prabavathi P, Rani SS. 2019. Design of frequency-signature based multiresonators using quarter wavelength open ended stub for chipless RFID tag. In Proceedings of the 2019 National Conference on Communications (NCC) (1–6).
54. Jalil ME, Rahim MKA, Samsuri NA, Dewan R. 2014. Chipless RFID tag based on meandered line resonator. In Proceedings of the 2014 IEEE Asia-Pacific Conference on Applied Electromagnetics (APACE) (203–206).
55. Babaeian F, Karmakar NC. 2020. Compact multi-band chipless RFID resonators for identification and authentication applications. *Electronics Letters*, 56(14), 724–727.
56. Janeczek K. 2017. Reliability analysis of UHF RFID tags under long-term mechanical cycling. *Microelectronics Reliability*, 75, 96–101.
57. Virkki J, Björninen T, Kellomäki T, et al. 2014. Reliability of washable wearable screen printed UHF RFID tags. *Microelectronics Reliability*, 54(4), 840–846.
58. Simorangkir RBVB, Le D, Bjorninen T, Sayem ASM, Zhadobov M, Sauleau R. 2019. Washing durability of PDMS-conductive fabric composite: realizing washable UHF RFID tags. *IEEE Antennas and Wireless Propagation Letters*, 18(12), 2572–2576.
59. Guibert M, Massicart A, Chen X, et al. 2017. Washing reliability of painted, embroidered, and electro-textile wearable RFID tags. In Proceedings of the 2017 Progress in Electromagnetics Research Symposium-Fall (PIERS-FALL) (828–831).
60. M. A. Islam, Y. Yap, N. C. Karmakar and AA. 2012. Compact printable orientation independent chipless RFID tag. *Progress In Electromagnetics Research C*, 33, 55–66.
61. Nayci Duman M, Usta I, Esmer GB. 2022. Effects of stitch density, thread tension and using conductive yarn as upper or lower thread on reading performance of embroidered RFID tag antennas. *Solid State Phenomena*, 333, 55–62.
62. Khan MUA, Raad R, Foroughi J, Tubbal F, Theoharis PI, Raheel MS. 2019. Effects of bending bow-tie chipless RFID tag for different polymer substrates. In Proceedings of the 2019 IEEE 13th International Conference on Signal Processing and Communication Systems (ICSPCS) (12–15).
63. Borisov BF, Charnaya E V., Radzhobov AK. 1994. Acoustic studies of LiKSO4 crystals in the 290 to 930 K region. *Physica Status Solidi (b)*, 181(2), 337–343.
64. Zhang M, Yeo TS, Li LW, Gan YB. 2006. Parallel FFT based fast algorithms for solving large scale electromagnetic problems. In Proceedings of the 2006 IEEE Antennas and Propagation Society International Symposium (3995–3998).